https://doi.org/10.1007/s41230-023-3003-8

Effect of heat treatment on microstructure, mechanical and tribological properties of in-situ (TiC+TiB)/TC4 composites by casting

***Bo-wen Zheng, Shuai Chen, Chun-yu Yue, Xue-jian Lin, Fu-yu Dong, Hong-jun Huang, Xiao-jiao Zuo, Yin-xiao Wang, and **Xiao-guang Yuan**

School of Materials Science and Engineering, Shenyang University of Technology, Shenyang 110870, China

Abstract: To enhance the performance of in-situ synthesized 6vol.% (TiC+TiB)/TC4 titanium matrix composites fabricated by casting, a variety of heat treatment processes were carried out. Upon conducting microstructure observations following various heat treatments, it was found that the composites exhibit a basketweave microstructure, consisting of an α phase and a transformed β phase. The sizes of (α+β) phases were found to be refined to varying degrees after the heat treatment processes, while the morphology of TiB remains largely unchanged and TiC becomes granulated. Compressive testing revealed that all composites subjected to different heat treatments demonstrate a notable increase in ultimate compressive strength as well as a slight improvement in plasticity compared to the as-cast state. The results of the tribological performance test indicated that the heat-treated composites exhibit lower average friction coefficient, specific wear rate, and worn surface roughness compared to the as-cast composite. Among the heat treatment processes studied, the composite solution heated at 1,150 °C/1 h followed by air cooling, then 950 °C/1 h followed by air cooling, and finally 500 °C/4 h followed by air cooling, demonstrates the highest levels of hardness, compressive strength, and wear resistance. These improvements are attributed to the combined effects of solid solution strengthening, grain refinement, and the pinning of dislocation slip.

Keywords: titanium matrix composites; heat treatment; mechanical properties; tribological properties

CLC numbers: TG146.23 **Document code:** A **Article ID:** 1672-6421(2023)03-207-11

1 Introduction

Titanium matrix composites (TMCs) have become increasingly popular in critical component applications in the aerospace, automotive, and defense industries due to their many advantages, including higher specific strength and stiffness than titanium alloys, as well as excellent corrosion resistance, high-temperature resistance, and wear resistance [1-6]. These materials are subject to stringent requirements for both structure and mechanical properties, as they must be able to withstand heavy loads and severe friction conditions [7-9]. To improve the strength and wear resistance of TMCs, most research focuses on selecting suitable reinforcements and determining the optimal amount of reinforcement to add [10-12]. However, these composites still exhibit sacrificial ductility, which can make subsequent processing more challenging. To address this issue, heat treatment has emerged as an effective way to optimize the performance of TMCs by regulating their phase transition behavior and microstructure, thereby enhancing their strength without sacrificing plasticity.

In discontinuously reinforced TMCs, in-situ TiB whiskers and TiC particles are highly regarded as ideal reinforcements due to their exceptional modulus and thermal stability. Furthermore, their nearly identical density and expansion coefficient to Ti make them a desirable choice for creating these composites [13-16]. The (TiC+TiB)/TC4 composites are prepared using the in-situ casting method, due to that TC4 (a Ti-6Al-4V series titanium alloy) exhibits excellent comprehensive properties and suitability for heat treatment strengthening [17-19]. Conventional heat treatment methods for titanium alloys include β heat treatment and α/β heat treatment, which are effective at enhancing creep properties but may result

***Bo-wen Zheng**

Male, born in 1989, Lecturer, master supervisor. His research interests mainly focus on microstructure control, mechanical properties and wear behavior of titanium alloys and titanium matrix composites.

E-mail: zhengbowen89@163.com

****Xiao-guang Yuan**

E-mail: yuanxg@sut.edu.cn

Received: 2023-01-06; Accepted: 2023-03-24

in reduced ductility [20-22]. However, a novel heat treatment process known as the TRIPLEX heat treatment has emerged [22]. This process involves solution treatment at both the β phase region and (α+β) phase region, followed by aging treatment. The TRIPLEX heat treatment is considered an effective method for improving both strength and plasticity [23]. Research indicates that TRIPLEX heat treatment can yield a dense basketweave microstructure in TMCs [24]. This microstructure can enhance not only tensile strength but also fracture toughness, fatigue crack propagation resistance, and creep resistance [25-27]. However, few studies have investigated the impact of TRIPLEX heat treatment on microstructure evolution and the resulting mechanical and tribological properties of TMCs. Thus, it is crucial to have a better understanding of the relationship between microstructure, mechanical properties, tribological characteristics, and various heat treatment processes, particularly for using TMCs in diverse working conditions, which demand high strength and wear resistance.

In this study, the conventional β heat treatment process and two types of TRIPLEX heat treatment processes were performed to evaluate their impacts on the microstructure, mechanical properties, and tribological properties of the (TiC+TiB)/TC4 composites.

2 Experimental procedures

2.1 Sample preparation

The experimental raw materials included commercial TC4 alloy, B_4C powder (98% purity, with an average particle size of 50 μm), and C powders (99.8% purity, with an average particle size of 5–7 μm). The 6vol.% (TiB+TiC) reinforced TC4 composites were prepared using a vacuum non-consumable arc melting furnace with argon protection, and the ratio of TiB to TiC is 1:1. To prevent splashing, the C powders and B_4C powders were wrapped in aluminum foil and placed in the crucible inside the furnace with the experimental materials before melting. To ensure material structure uniformity, all the prepared samples need to be melted for 5 times, and cooled in a water-cooled copper crucible to form a button ingot weighing around 30 g. The following in-situ reactions occurred in the melts [28]: $5Ti+B_4C=4TiB+TiC$ and $Ti+C=TiC$.

2.2 Determination of heat treatment process

A theoretical calculation method was used to determine the β transition temperature of the (TiC+TiB)/TC4 composites accounting for the influence of various elements. The calculation equation is as follows:

$$A_{c3}=885\ ^{\circ}C+\Sigma E_i\times\Delta t \quad (1)$$

where A_{c3} is the β transition temperature of TMCs, and 885 °C is the β transition temperature of pure titanium; E_i refers to element content, Δt is the change in phase transition point caused by corresponding element. The effect of each element on the phase transformation point of the titanium alloy is listed in Table 1. The chemical composition of the TC4 alloy was detected by X-ray fluorescence spectrometer (ARL PERFORM' X), as shown in Table 2. Based on Eq. (1), the β phase transition point of the (TiC+TiB)/TC4 composites designed in this study was calculated to be 1,030 °C.

The grain size and nucleation quantity of TC4 alloy are influenced by the β heat treatment temperature, and the heat treatment temperature in the α+β region is approximately 100 °C below the phase transition point [30]. The aging process of TC4 alloy involves heating to around 500–600 °C, followed by holding for 4–12 h [31]. Therefore, based on the measured β phase transition point, the two β heat treatment temperatures of 1,050 °C and 1,150 °C were set to study the effect of solution temperature on microstructure and properties. The heat treatment temperature in the α+β region was set to 950 °C, and the aging temperature was set at 500 °C. The detailed heat treatment processes of the conventional β heat treatment and two β-three stages heat treatments are displayed in Table 3. To ensure a high-vacuum environment during the heat treatment, the samples were sealed in a quartz tube.

2.3 Mechanical properties and friction tests

The compression properties were tested using an MTS810 electronic universal testing machine at a strain rate of 1.38×10^{-4} s^{-1} at room temperature. The samples measured Φ3 mm×6 mm in size.

Table 1: Effect of element on phase transition point of titanium alloy [29]

Element type	Element	Element content (wt.%)	Change in phase transition point/Element amount
α stable element	Al	0–2	+14.5 °C/1.0wt.%
		2–7	+23.0 °C/1.0wt.%
	C	0–0.15	+2.0 °C/0.01wt.%
		0.15–0.5	+0.15 °C/0.01wt.%
	B	0–0.05	+1 °C/0.01wt.%
		0.05–0.5	+0.025 °C/0.01wt.%
	O	0–1.0	+2.0 °C/0.01wt.%
	N	0–0.50	+5.5 °C/0.01wt.%
β stable element	V	0–10	−14.0 °C/1.0wt.%
	Mo	0–5	−5.5 °C/1.0wt.%
	Nb	0–10	−8.5 °C/1.0wt.%
	Si	0.45–1	−3.5 °C/0.1wt.%
	H	0–0.50	−5.5 °C/0.01wt.%
	Fe	0–15.0	−16.5 °C/1.0wt.%
Neutral element	Zr	0–10	−2.0 °C/1.0wt.%

Table 2: Composition of TC4 alloy (wt.%)

Al	V	Fe	Si	Ti
6.1	4.2	0.05	0.08	Bal.

Table 3: Heat treatment processes for (TiC+TiB)/TC4 composites

Heat treatment process	β region	α+β region	Aging
HT1	1,050 °C/3 h+AC	–	500 °C/4 h+AC
HT2	1,050 °C/1 h+AC	950 °C/1 h+AC	500 °C/4 h+AC
HT3	1,150 °C/1 h+AC	950 °C/1 h+AC	500 °C/4 h+AC

The results were the average of at least three measurements. The hardness of the composites was measured using an HR-150A-type Rockwell hardness tester under a 1,000 g load holding for 15 s. The final hardness value was determined by taking the average of the five indentation points.

The MMU-5G friction tester was used to conduct the dry friction testing in a pin-on-disc contact configuration with a sliding mode. The testing was performed with a load of 150 N and a sliding speed of 0.55 $m \cdot s^{-1}$ for 10 min. As the counter-abrasive pair, Cr12MoV steel (58-60HRC) was selected. The samples were machined to cylindrical pins measuring Φ4 mm×15 mm. All friction tests were conducted a minimum of three times, and the final specific wear rate was calculated as the average value of these tests. To ensure accuracy, an ultrasonic cleaning machine was used to clean all samples in acetone and remove any residual debris on worn surfaces. The specific wear rate of the samples was then determined using the following equation:

$$W = \frac{V}{FS} \tag{2}$$

where W is the specific wear rate, V is the wear volume of pins (mm^3), S is the sliding distance (m), and F is the normal load (N).

2.4 Microstructure characterization

XRD analysis was performed using a Shimadzu XRD-7000 type X-ray diffractometer. The microstructure of the composites were observed using a S-3400N scanning electron microscope. The microstructure and element distribution of the worn surface of the composites were detected using a thermal field emission scanning electron microscope (ZEISS, Gemini SEM 300). Laser scanning confocal microscopy (LSCM, OLS4100, Japan) was used to obtain the image of worn surface topography. Meanwhile, an accurate numerical description of the three-dimensional (3D) worn surface was obtained.

To obtain crystallographic information such as grain boundary distribution, grain size and orientation of the composites, the microstructure was characterized by electron backscattered diffraction (EBSD) with a step size of 0.5 μm. The EBSD data was analyzed using the Channel 5 HKL software from Oxford Instruments Inc., UK. Before analysis, the EBSD samples were mechanically ground and then electropolished in a solution consisting of 6% $HCLO_4$, 34% $CH_3(CH_2)_3OH$, and 60% CH_3OH. The polishing process was conducted at around –25 °C with an applied potential of 30 V for 20 s.

3 Results and discussion

3.1 Microstructure

Figure 1 shows the X-ray diffraction patterns of (TiC+TiB)/TC4 composites under different states. It indicates the presence of TiC and TiB phases in addition to Ti base. Compared with as-cast composites, the β-Ti peaks of the composites with HT1 and HT3 decrease significantly at 38.48° and 76.68°, while the β-Ti peaks of the composites with HT2 increase, which is attributed to the transition from β-Ti to α-Ti after heat treatment. Compared with HT2, HT1 has a longer solid solution time, and HT3 has a higher solid solution temperature. Consequently, the Ti peaks of HT1 and HT3 composites undergo a more thoroughly transition from β-Ti to α-Ti, resulting in a significant decrease in β-Ti peaks.

Figure 2 shows the microstructures of the composites under different states. The microstructure analysis of the as-cast composites [Fig. 2(a)] reveals that the α-grains are lamellar in shape, and the needle-like TiB and nearly granulated TiC particles are uniformly distributed near the β-grain boundaries. Following the HT1 heat treatment, it is observed that the α-grains become nearly equiaxed. This can be attributed to the diffusion and diffusion-controlled phase transitions. The diffusion process is accelerated during the heat treatment, which reduces the anisotropy of diffusion in the α-grains, thereby facilitating the equiaxation of the α-grain. The α-phase precipitation process is a process of nucleation and growth [32]. The nucleation site, number of nuclei, and growth rate are dependent on the composition and cooling conditions of the alloy. The rapid air-cooling rate during the cooling stage results in an increase in both nucleation site and number of nuclei. Meanwhile, the α-phase nucleates within the grain and then grows into independent lamellae due to the rapid air-cooling rate. The lamellae restrict each other, preventing them from growing into coarse grains [33]. Furthermore, the β to α transformation is not complete, resulting in a small amount of transformed β distributed among the α phase, forming a basketweave structure with a uniform distribution of α and transformed β phases. This structure is beneficial for enhancing the fracture toughness and preventing fatigue crack extension of TMCs [34]. After HT1 heat treatment, the morphology of TiB remains basically unchanged, while TiC gradually granulates. Additionally, some of the TiC particles dissolve in the matrix [Fig. 2(b)].

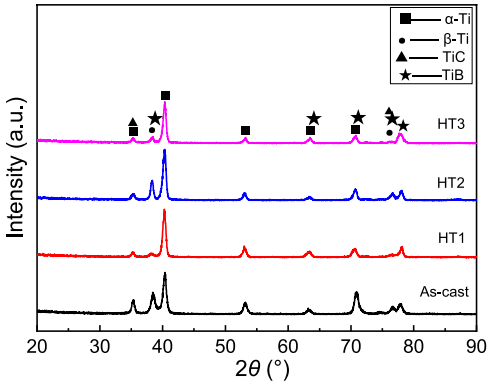

Fig. 1: XRD patterns of the composites under different states

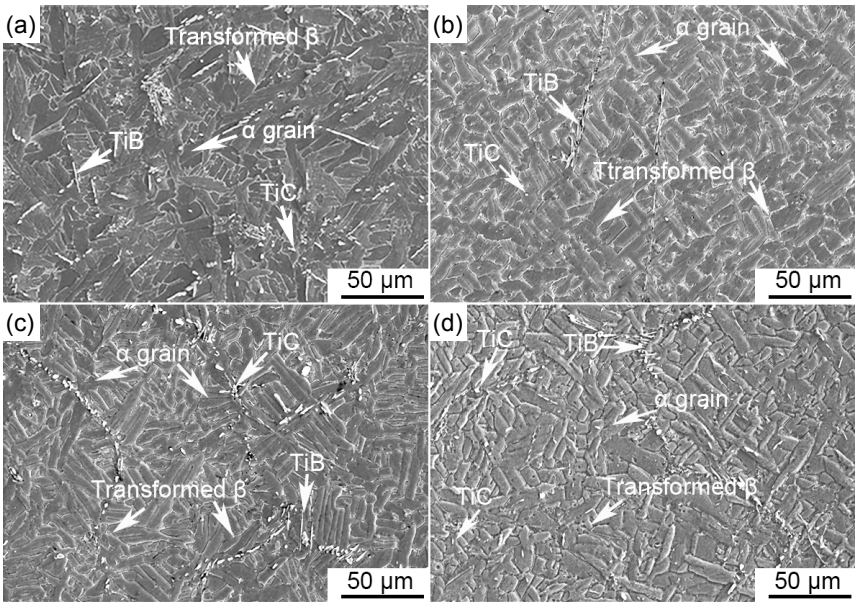

Fig. 2: SEM images of (TiC+TiB)/TC4 composites under different states: (a) as-cast; (b) HT1; (c) HT2; and (d) HT3

Regarding the (TiC+TiB)/TC4 composites after HT2 heat treatment, the phase transformation occurs in three stages. In the first stage, the transformation is β→α+sub-stable β. In the second stage, the transformation is sub-stable β→α+β during heating and β→α+sub-stable β during air cooling. In the third stage, the transformation is also sub-stable β→α+β. Compared with HT1, the number of reinforcements after HT2 [Fig. 2(c)] is slightly increases due to the shorter solid solution time than HT1.

The solid solution temperature in the first stage of HT3 is 1,150 °C, which is 100 °C higher than that of HT2. The basketweave structure shown in Fig. 2(d) consists of α phases and a small amount of transformed β. TiC undergoes a change in morphology from short rod to granule mainly due to the varying radii or positions between adjacent TiC particles. This produces a chemical potential difference, which generates a driving force that promotes solute atoms to diffuse from a smaller radius curvature to a larger radius. As a result, the morphology of TiC gradually changes to granular due to the diffusion of C atoms[35]. Thus, the higher solid solution temperature in the first stage accelerates the diffusion process and promotes the granulation of TiC. After heat treatment, the morphology of TiB remains basically unchanged. This is because heat treatment can change the morphology of TiB precipitates formed by solid-state reaction, but, it has no effect on the morphology of TiB whiskers formed during solidification [36].

To further investigate the microstructure evolution of the matrix and reinforcements, the EBSD images are shown in Fig. 3. The low angle grain boundaries (LAGBs) (2–15°) are marked in red, and high angle grain boundaries (HAGBs) (>15°) are marked in blue [Figs. 3(a_1)–(d_1)]. For as-cast composites, the proportion of [0001] oriented grains is high, the distribution of the [$\bar{1}2\bar{1}0$] and [0001] oriented grains is relatively uniform, and only a few [$01\bar{1}0$] oriented grains can be found [Fig. 3(a_2)]. The average size of the α-grains is about 12 μm, with approximately 26.33% of the grains measuring less than 5 μm, and 45.91% of the grains measuring between 5 μm and 10 μm [Fig. 3(a_3)]. Additionally, the proportion of LAGBs is relatively low, while the proportion of HAGBs is high [Fig. 3(a_4)].

After HT1 heat treatment, the proportion of [$01\bar{1}0$], [$\bar{1}2\bar{1}0$] and [0001] oriented grains is relatively uniform without a preferential orientation [Fig. 3(b_2)]. The average size of α-grains is decreased to 5.355 μm, and the ratio of α-grains below 5 μm increases to 65.10% [Fig. 3(b_3)]. The proportion of LAGBs is 10.9%, while that of HAGBs is 70.6% [Fig. 3(b_4)]. This indicates that the grain orientation distribution becomes more uniform and the grain is refined after HT1 heat treatment.

For the composites with HT2 heat treatment, the proportion of [$\bar{1}2\bar{1}0$] oriented grains is higher, and the grains grown along the [0001] and [$01\bar{1}0$] orientations are well-distributed [Fig. 3(c_2)]. Similarly, the average grain size is decreased to 5.406 μm, of which approximately 51.76% are α-grains below 5 μm, and 36.89% are between 5 μm and 10 μm [Fig. 3(c_3)]. Compared with HT1, the solution time of HT2 is shorter. As a result, the equiaxed particles formed by TiC melting are less, and the effect of TiC dispersion on grain refinement is smaller. Therefore, the grain size after HT2 heat treatment is larger than that after HT1 heat treatment. In addition, compared with as-cast and HT1, the content of HAGBs is increased, accounting for 80.8%, while the proportion of LAGBs is decreased, accounting for 11.8% [Fig. 3(c_4)].

After HT3 heat treatment, the distribution of [$\bar{1}2\bar{1}0$], [0001] and [$01\bar{1}0$] oriented grains appear to be more evenly distributed than the other treatments. Additionally, the average size of the α-grain is the smallest at 4.976 μm. There is also a higher percentage of HAGBs in comparison to the as-cast, HT1, and HT2 treatments, reaching a percentage of 81.6% [Figs. 3(d_3) and (d_4)]. Overall, HT3 heat treatment is considered to have the most ideal refinement effect.

The phase fractions of composites under different states were also analyzed by EBSD analysis software, as listed in Table 4. It can be found that after heat treatment, the content of α phase increases, while that of the β phase slightly decreases. The content of TiC also decreases. While, the content of TiB is basically unchanged.

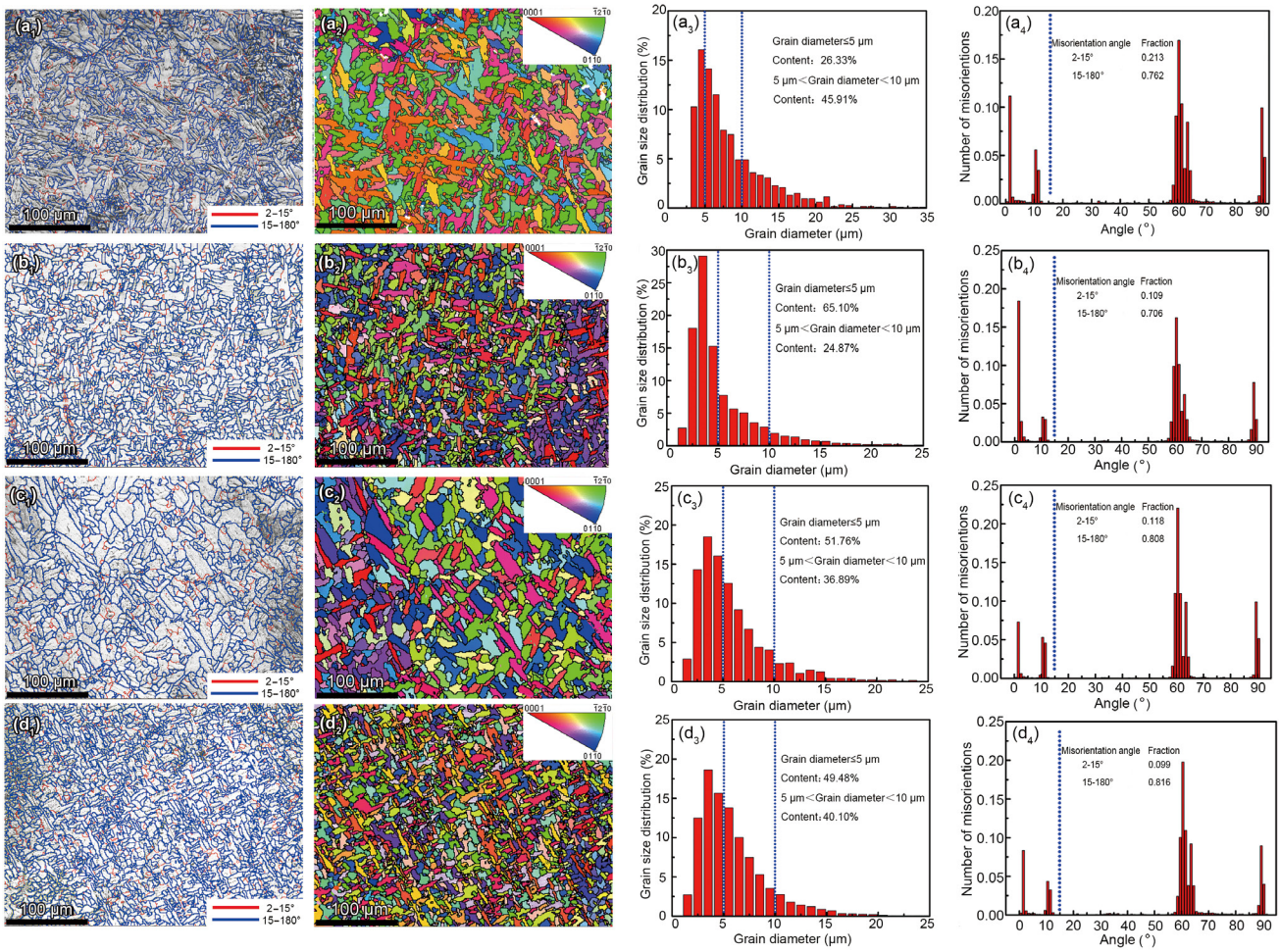

Fig. 3: EBSD analysis of (TiC+TiB)/TC4 composites under different states: (a_1–d_1) grain boundary (GB) maps; (a_2–d_2) inversed pole figure (IPF); (a_3–d_3) grain size distributions; (a_4–d_4) grain misorientation

Table 4: Fraction of different phases in (TiC+TiB)/TC4 composites under different states

State	α phase (%)	β phase (%)	TiC (%)	TiB (%)
As-cast	93.53	0.38	3.15	2.94
HT1	94.03	0.27	2.77	2.93
HT2	93.83	0.33	2.88	2.96
HT3	94.28	0.21	2.62	2.89

3.2 Mechanical properties of (TiC+TiB)/TC4 composites under different states

Figure 4 shows the Rockwell hardness of the (TiC+TiB)/TC4 composites under various heat treatment processes. The hardness of the (TiB+TiC)/TC4 as-cast and after HT1, HT2, and HT3 heat treatments are 52.8, 53.4, 53.8, and 53.9 HRC, respectively. The hardness of the composites is increased by heat treatments.

Figure 5 shows the compression curve of the (TiC+TiB)/TC4 composites under different states. It can be seen that the strength and plasticity of the composites after heat treatment are improved compared with the as-cast one, except for the composites with HT2. The composites with HT3 have the best compression strength and compression plasticity. After heat treatment, the grain size of the composites decreases to a certain extent. Based on the Hall-Petch formula, the crystal interface is the obstacle of dislocation movement, thus the smaller the grains, the more the grain boundaries there are, the more the dislocation is anchored, and then the higher the strength of the composites [37]. In addition, during compressive deformation, the deformation can be dispersed to more grains, producing more uniform deformation without local stress concentration. This leads to an increase in compressive plasticity. For HT1 and HT3, the higher heat treatment temperature in the β-phase zone of HT3 or the longer holding time of HT1 compared to HT 2 results in the stronger diffusion ability of C

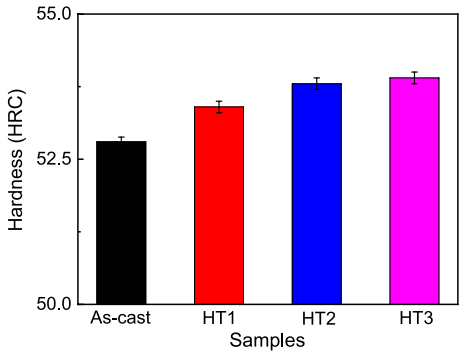

Fig. 4: Hardness of (TiC+TiB)/TC4 composites under different states

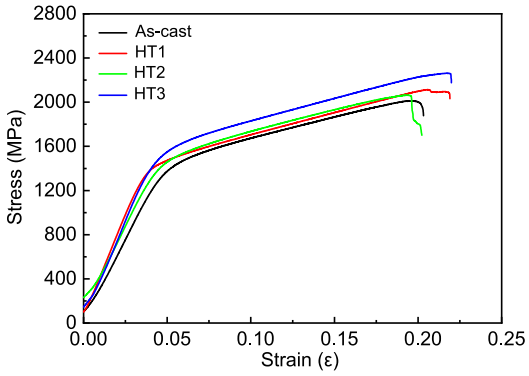

Fig. 5: Compression curves of (TiC+TiB)/TC4 composites under different states

atoms, thus TiC can quickly achieve granulation. After granulation, TiC can bear high stress and blunt the crack tip, thereby preventing premature fracture during compression and improving mechanical properties. HT2 has a shorter heat treatment time in the β-phase zone compared to HT1, and a lower heat treatment temperature in the β-phase zone compared with HT3. This results in a lower degree of TiC granulation, and thus a lower compressive plasticity.

Figure 6 illustrates the fracture morphology of the (TiC+TiB)/TC4 composites under different states after the compression testing. The number of dimples on the fracture surface of the composites after heat treatment is significantly more than that of as-cast one [Fig. 6(a)], indicating that the composites after heat treatment have better compression plasticity. In addition, it can be seen from Figs. 6(b) to (d) that many large and shallow dimples appear on the fracture surface along with some narrow and deep pits. During deformation, the formation of these deeper pits on the fracture surface is usually accompanied by the fracture of the brittle second phase [38, 39]. The relatively hard reinforced phase with strong interface adhesion deforms with the matrix. However, due to the brittleness of the reinforced phases, they may break and form pits as the matrix continues to deform. Due to the strong interfacial binding force, the cavities formed by the fracture of the reinforced phase grow through plastic deformation, forming small and deep pits. The strong interfacial binding force of the reinforced phase indicates their stable bond with the matrix, thus ensuring the effective transfer of load.

3.3 Tribological properties of (TiC+TiB)/TC4 composites under different states

Figure 7 shows the coefficient of friction (COF) of the (TiC+TiB)/TC4 composites under different states. The COF curves go through two stages: the run-in stage and the stable stage. After a short run-in stage, all of the samples quickly enter the stable stage. The average COFs of the (TiC+TiB)/TC4 composites before and after the heat treatments are 0.264, 0.259, 0.258 and 0.262, respectively. After heat treatment, the COF is reduced due to the higher strength and surface hardness. This accords with the Archard theory [40].

Figure 8 shows the specific wear rate of the (TiC+TiB)/TC4 composites under different states. Heat treatment decreases the specific wear rate and improves the wear resistance of the composites, but the extent of improvement in wear resistance varies slightly with different heat treatments, which should be related to the microstructure and worn surface state of the composites.

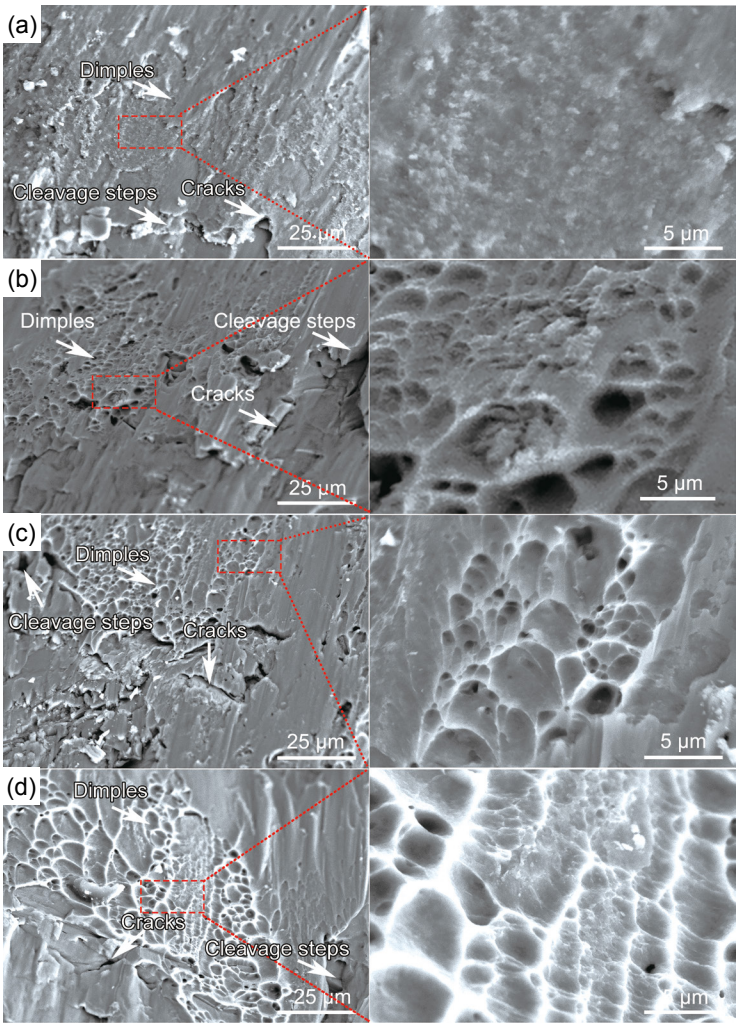

Fig. 6: Compressive fracture fractographs of (TiC+TiB)/TC4 composites under different states: (a) as-cast; (b) HT1; (c) HT2; and (d) HT3

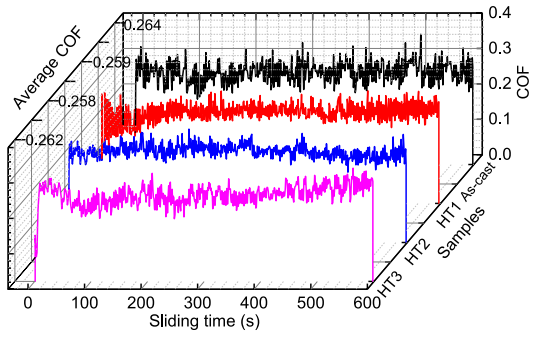

Fig. 7: Coefficient of friction of (TiC+TiB)/TC4 composites under different states

To analyze the effect of heat treatment on worn surfaces, 3D surface morphology was conducted by laser scanning confocal microscopy to determine the wear tracks on the composites under different states, as displayed in Fig. 9. It can be found that different degrees of wear tracks exist on the worn surface of the as-cast composites. Some deep furrows are seen on the worn surface, which has a maximum surface roughness (S_a) of 4.03 μm [Fig. 9(a)]. Compared with the as-cast composites, the wear tracks decrease to different degrees after heat treatment. After HT1 heat treatment, S_a of the furrow decreases to 2.05 μm [Fig. 9(b)]. The S_a of the composites after HT2 heat treatment is 2.73 μm [Fig. 9(c)]. Moreover, only small scratches and furrows are detected on the worn surface of the composites after HT3 heat treatment, and the S_a is further decreased to 2.25 μm [Fig. 9(d)].

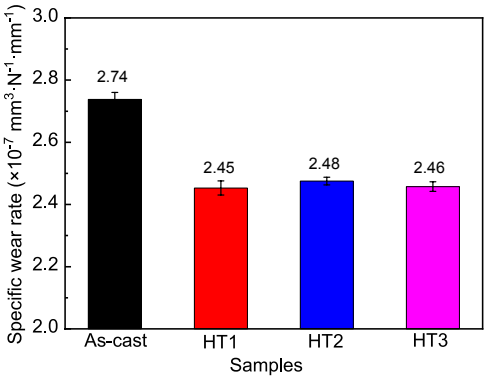

Fig. 8: Specific wear rate of (TiC+TiB)/TC4 composites under different states

Figure 10 shows the worn morphology and element distribution of the (TiC+TiB)/TC4 composites under different states. A large delamination and deep furrow are detected on the worn surface of the as-cast composites [Fig. 10(a)]. They are significantly reduced after HT1 heat treatment, indicating improvement in wear resistance [Fig. 10(b)]. After HT2 heat treatment, the amount of furrow and delamination on the worn surface is slightly higher than that of HT1 and as-cast ones [Fig. 10(c)]. Only a few minor delaminations and furrows are observed on the worn surface after HT3 heat treatment [Fig. 10(d)]. After heat treatment, the surface strength and hardness are higher, the shear resistance is improved, and large

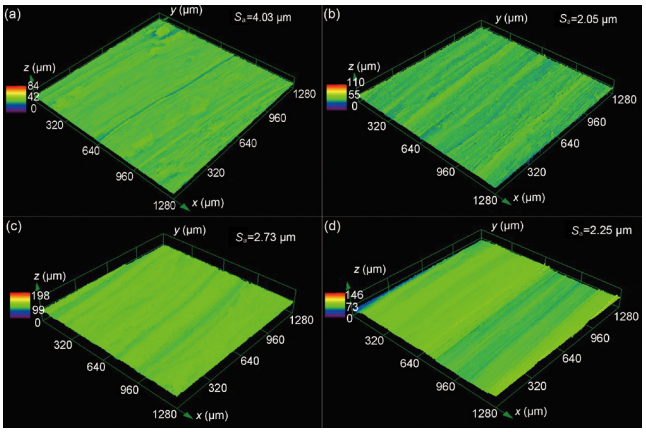

Fig. 9: 3D wear track of (TiC+TiB)/TC4 composites under different states: (a) as-cast; (b) HT1; (c) HT2; and (d) HT3

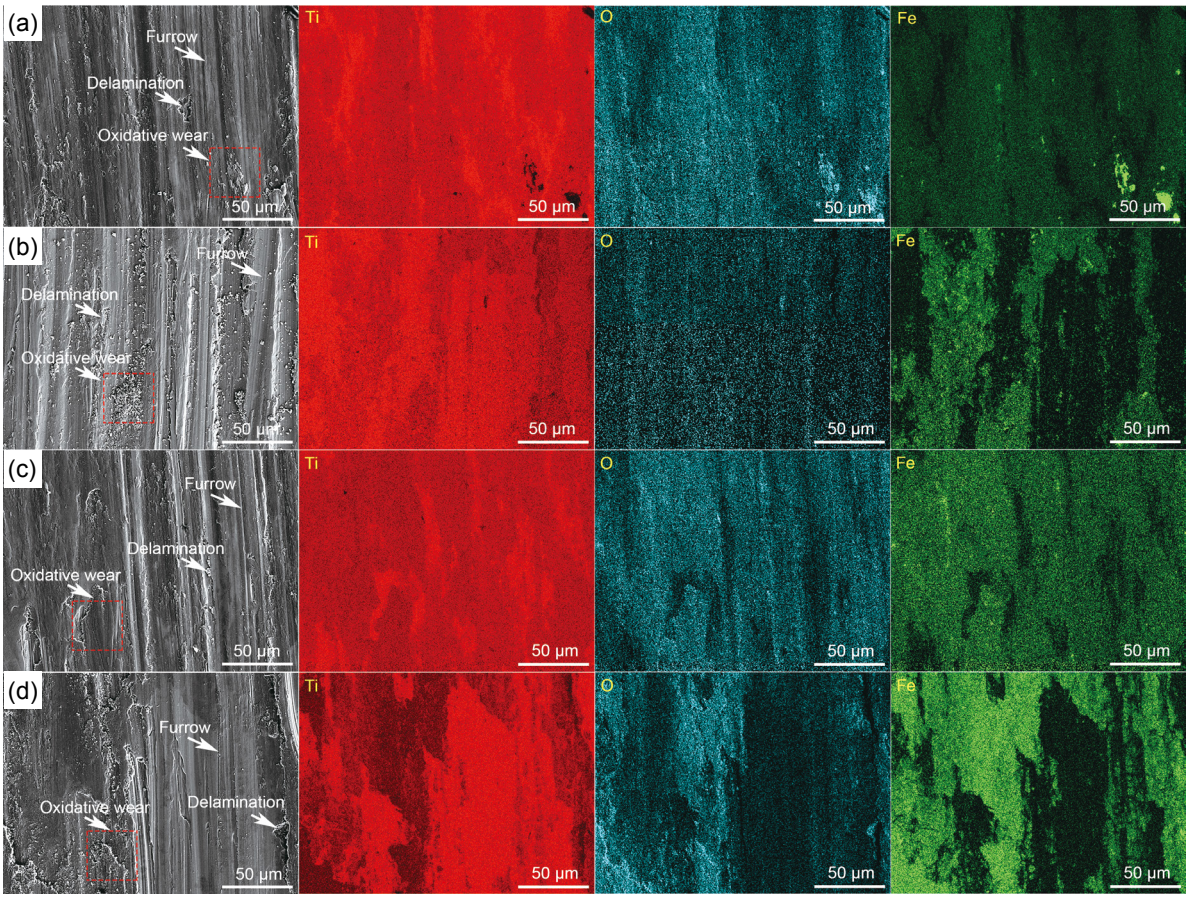

Fig. 10: Worn morphology analysis of (TiC+TiB)/TC4 composites under different states: (a) as-cast; (b) HT1; (c) HT2; and (d) HT3

peeling less likely to occur [41]. The wear mechanism of the (TiC+TiB)/TC4 composites after heat treatment is abrasive wear, among which the wear resistance after HT1 heat treatment is the optimum, followed by HT3, and then HT2. All the composites shows better wear resistance than the as-cast one. According to EDS analysis, the Fe and O elements are found on the worn surface, which indicates that a certain amount of friction oxide is formed on the worn surface during the friction process. From surface scanning, it can be seen that the oxide distributed on the worn surface increases after heat treatment. The plow marks and a small amount of peeling and oxidation wear marks along the sliding direction can be clearly observed on the worn surface of the as-cast composites. In addition, the content of Fe on the worn surface is low, and no dense tribo-layer exists on the worn surface. Compared with the as-cast worn surface, more Fe is transferred from the counter pair to the worn surface after heat treatment. They are combined with the matrix to form a continuous and dense tribo-layer to protect the matrix.

Figure 11 indicates the cross-sectional morphology and EDS line analysis of worn surfaces of the (TiC+TiB)/TC4 composites before and after heat treatment. It can be found that a continuous dense tribo-layer with a thickness of about 20 μm exists on the worn surface, along with a small plastic deformation zone on the worn sub-surface of as-cast composites [Fig. 11(a)]. The presence of Fe oxides is detected on the tribo-layer according to the EDS line scan analysis of the HT1 composites [Fig. 11(b)]. A tribo-layer about 15 μm thick is formed on the worn surface, and a larger plastic deformation zone exists on the sub-surface. Similarly, Fe oxides are found on the tribo-layer of the HT2 composites [Fig. 11(c)]. For the HT3 composites, it can be found that there is a tribo-layer about 8 μm thick on the worn surface, and a small plastic deformation zone on the worn sub-surface. The EDS result also indicates the existence of oxides [Fig. 11(d)].

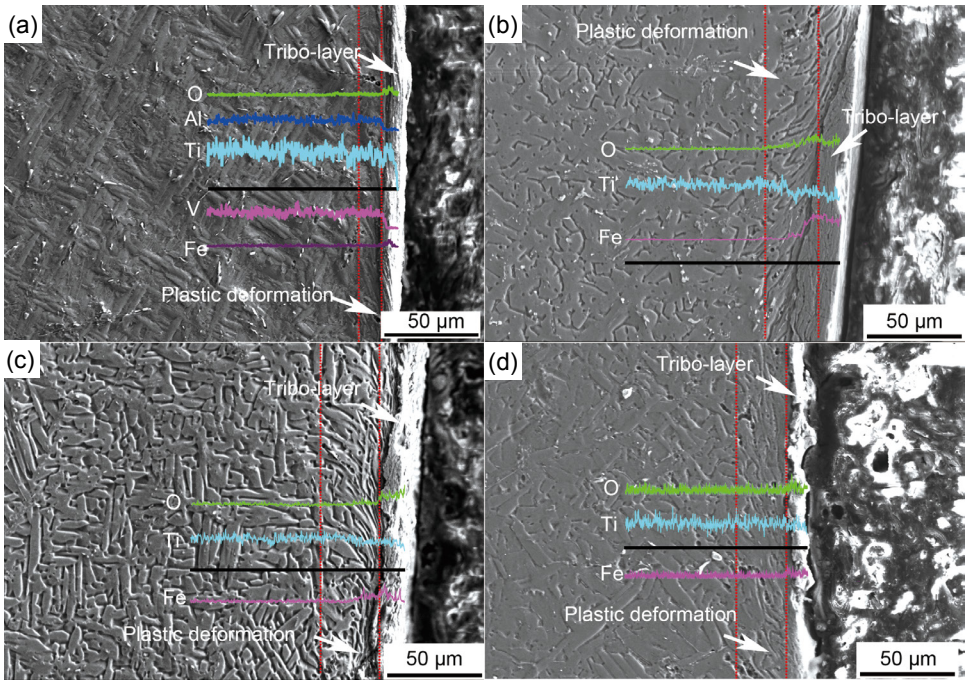

Fig. 11: EDS analysis for worn cross-sectional surfaces of (TiC+TiB)/TC4 composites under different states: (a) as-cast; (b) HT1; (c) HT2; and (d) HT3

The formation of a tribo-layer on a worn surface is closely related to the generation of wear debris. During sliding wear, high temperature, heavy load, and friction shear contribute to the production of wear debris. Some of the debris is expelled from the friction system due to centrifugal force, while the rest accumulates on the worn surface and becomes compacted, eventually forming a tribo-layer that contains a high concentration of oxygen. The tribo-layer formed on the worn surface plays the role of protecting the matrix, thus reducing wear rate [42]. In addition, the TiC and TiB reinforcements with high hardness and high thermal conductivity can effectively improve the heat resistance and thermal conductivity of the composites [43]. The friction heat generated by the worn surface can be rapidly released to prevent the matrix from softening due to high surface temperature. This helps to inhibit sub-surface deformation caused by frictional shear stress, thereby reducing damage to worn surfaces and minimizing the reduction of COF [44].

Figure 12 exhibits the XRD patterns of the worn surfaces of the (TiC+TiB)/TC4 composites under different states. The worn surface mainly contains the Ti matrix, TiB, TiC, TiO_2, FeO, and Fe_2O_3 oxides. Element Fe is not present in any of the composites, but only in the counter-abrasive disc. This suggests that the transfer of Fe element occurs during friction. With the increase of the temperature of the worn surface, the Ti and Fe elements on the surface are easily oxidized to form oxides. The presence of TiO_2, FeO, and Fe_2O_3 oxides in the dense tribo-layer is conducive to preventing direct interaction of the contact surfaces and forming three-body wear [45]. This helps to improve the wear resistance of the composites.

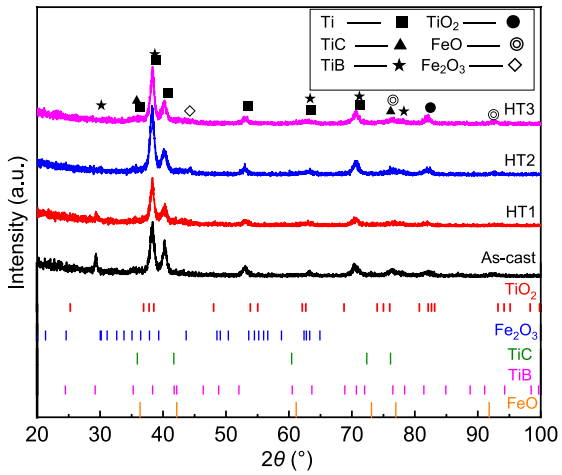

Fig. 12: XRD analysis for worn surface of (TiC+TiB)/TC4 composites under different states

3.4 Strengthening and toughening mechanisms

Figure 13(a) shows a schematic diagram of the microstructure evolution of the (TiC+TiB)/TC4 composites after different heat treatments, and the illustrations of crack propagation caused by compression. Compared with the conventional solution of HT1, the HT2 heat treatment undergoes a second stage of solution in the α+β region. This double high-temperature solution causes the α phase to continuously grow, resulting in an increase of the length-diameter ratio of the α grain [46, 47]. The content and size of the α phase during the TRIPLEX heat treatment process depend mainly on the solution temperature of the first and second stages. If the solution temperature of the first stage is low, a part of the α phase may not convert into the β phase. During the subsequent heat treatment and aging process, the α phase and metastable β phase obtained during the cooling process at the first stage will decompose, grow, and merge, forming relatively coarse α lamellae. In addition, if the solution temperature at the first stage increases, the thermal activation energy rises, which promotes the transformation of α → β. This leads to a decrease in the content of the large size α phase. In the second solution stage, the α phase continues to change into the β phase. During the cooling process below the β transition temperature, the α phases nucleate at the β grain boundaries, as well as at sites provided by TiB and TiC [48]. As a result, the α phases continue to grow until they encounter other α lamellae. The combination of a smaller β grain size and additional nucleation sites leads to a significant reduction in the α size. Therefore, for the HT3 heat treatment, the higher solution temperature in the first stage causes more α phase to change into the β phase. During the second stage of solution, the α phase continues to transform into the β phase, resulting in a finer α phase after air cooling. Subsequently, the fine α phase and transformed β phase interlace during aging, forming a basketweave microstructure.

In order to analyze the synergistic reinforced mechanism of the (TiC+TiB)/TC4 composites, the illustrations of crack propagation during compression deformation are displayed in Fig. 13(b). The low plasticity of as-cast composites is mainly due to the formation of a large-sized α phase and the uneven distribution of reinforced phases [49]. It is well known that the α phase (hcp) possesses a higher strength but lower ductility compared with β phase (bcc). Therefore, the distribution and size of the α phase have an important influence on the fracture behavior of the composites [50]. After HT3 heat treatment, the denser basketweave microstructure and higher interweaving of α phase lead to more dislocation tangles, resulting in increased fracture toughness and resistance to crack propagation [51]. The blunting of cracks delays the compression fracture process, and the boundary crack caused by the aggregation of TiB/TiC is one of the reasons for the cracking of the composites. The uneven distribution and local aggregation of reinforced phases in the as-cast composites can cause debonding during deformation, introducing vacancies and other defects that lead to crack initiation and propagation [52]. After HT3 heat treatment, the distribution of reinforced phases is more uniform, the crack initiation and propagation caused by local aggregation of reinforced phases are reduced. In addition, for a period of crack propagation, the TiB whiskers can bridge and change the direction of crack propagation, preventing crack propagation [53]. The spherical TiC particles can effectively bear the load during compression, reducing crack nucleation and propagation so that the composites can obtain higher strength and fracture toughness [54].

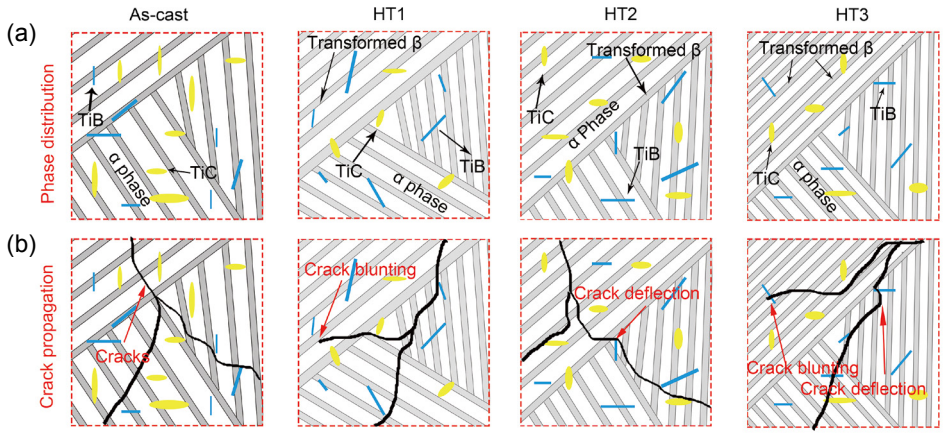

Fig. 13: Schematic diagram of microstructure evolution (a) and crack propagation (b) after different heat treatments

4 Conclusions

(1) Compared with the as-cast (TiC+TiB)/TC4 composites, the α grains of the composites after heat treatments are refined in different degrees, and the proportion of HAGBs increases. Among the three heat treatments, the grain refinement efficiency of the composite with HT3 (solution treated at 1,150 °C for 1 h, followed by solution treated at 950 °C for 1 h, and aged at 500 °C for 4 h) is the most obvious. As the solid solution temperature increases, the TiC particles become more granulated. However, the TiB particles do not show significant changes and maintain good bonding with the matrix.

(2) After heat treatment, the hardness of the (TiC+TiB)/TC4 composites slightly increases. The compressive strength also shows a significant increase from 1,821.90 MPa in the as-cast condition to 2,262.06 MPa in the HT3 condition. Additionally, heat treatment improves the compressive plasticity of the composites, except for HT2 where there is a slight decrease.

(3) The friction coefficient and specific wear rate of the (TiC+TiB)/TC4 composites are reduced to different degrees after different heat treatments, the average friction coefficient decreases from 0.264 to 0.259, 0.258, and 0.262, and the specific wear rate decreases from 2.74×10^{-7} to 2.45×10^{-7}, 2.48×10^{-7}, and 2.46×10^{-7} $mm^3\cdot N^{-1}\cdot mm^{-1}$, respectively.

(4) After heat treatment, the wear degree of the worn surface is reduced, and only a small amount of furrow and delamination exist on the worn surface. The wear mechanism after heat treatment is slight abrasive wear and oxidation wear.

(5) Coordinated deformation occurs among the α phase, β phase, TiB whiskers, and TiC particles. The formation of a basketweave microstructure can effectively improve deformation ability and delay fracture of the composites. Furthermore, the uniformly distributed reinforced phases can play a significant positive role in enhancing the bear capacity and strengthen the composites.

Acknowledgement

This study was financially supported by the Scientific Research Fund of Liaoning Provincial Education Department, China (No. LJKZ0122).

Conflict of interest

The authors declare that they have no conflict of interest.

References

[1] Tian N, Dong L L, Wang H L, et al. Microstructure and tribological properties of titanium matrix nanocomposites through powder metallurgy using graphene oxide nanosheets enhanced copper powders and spark plasma sintering. Journal of Alloys and Compounds, 2021, 867: 159093.

[2] Li C Z, Fu B G, Dong T S, et al. Microstructure and dry sliding wear behavior of as-cast TiC_p/Ti-1100-0.5Nb titanium matrix composite at elevated temperatures. China Foundry, 2020, 17(6): 455–463.

[3] Banerjee D, William J C. Perspectives on titanium science and technology. Acta Materialia, 2013, 61(3): 844–879.

[4] Ghosh A, Sivaprasad S, Bhattacharjee A, et al. Microstructure fracture toughness correlation in an aircraft structural component alloy Ti-5Al-5V-5Mo-3Cr. Materials Science and Engineering: A, 2013, 568(15): 61–67.

[5] Ahmed M, Sawakin D G, Ivasishin O M, et al. The effect of ageing on microstructure and mechanical properties of powder Ti-5Al-5Mo-5V-1Cr-1Fe alloy. Materials Science and Engineering: A, 2014, 605(27): 89–97.

[6] Zhao E T, Chen Y Y, Kong F T, et al. Effect of yttrium on microstructure and mold filling capacity of a near-alpha high temperature titanium alloy. China Foundry, 2013, 10(4): 344–348.

[7] Xiao L, Lu W, Yang Z, et al. Effect of reinforcements on high temperature mechanical properties of in situ, synthesized titanium matrix composites. Materials Science and Engineering: A, 2008, 491(1): 192–198.

[8] Zhang Z G, Qin J, Zhang Z W, et al. Microstructure effect on mechanical properties of in situ, synthesized titanium matrix composites reinforced with TiB and La_2O_3. Materials Letters, 2010, 64(3): 361–363.

[9] Zhou Z G, Liu Y Z, Liu X H, et al. Constructing targeted bi-lamellar microstructure via heat treatment for high compressive strength and plasticity in selective laser melted Ti6Al4V-5vol%TiB composite. Materials Science and Engineering: A, 2022, 844: 143173.

[10] Zhou Z G, Liu Y Z, Liu X H, et al. Microstructure evolution and mechanical properties of in-situ Ti6Al4V-TiB composites manufactured by selective laser melting. Composites: Part B, 2021, 207: 108567.

[11] Zhang Q, Sun W B, Xu S L, et al. Nano-TiB whiskers reinforced Ti-6Al-4V matrix composite fabricated by direct laser deposition: Microstructure and mechanical properties. Journal of Alloys and Compounds, 2022, 922: 166171.

[12] Hayat M D, Singh H, He Z, et al. Titanium metal matrix composites: An overview. Composites: Part A, 2019, 121: 418–438.

[13] Chen K M, Zhang Q Y, Li X X, et al. Dry sliding wear behavior of TC11 alloy/GCr15 steel tribo-pair. Rare Metal Materials and Engineering, 2015, 44(6): 1531–1535.

[14] Caha I, Alves A C, Kuroda P A, et al. Degradation behavior of Ti-Nb alloys: Corrosion behavior through 21 days of immersion and tribocorrosion behavior against alumina. Corrosion Science, 2020, 167: 108488.

[15] Li H, Jia D C, Yang Z H, et al. Effect of heat treatment on microstructure evolution and mechanical properties of selective laser melted Ti-6Al-4V and TiB/Ti-6Al-4V composite: A comparative study. Materials Science and Engineering: A, 2021, 801: 140415.

[16] Li J, Zhou J, Feng A, et al. Investigation on mechanical properties and microstructural evolution of TC6 titanium alloy subjected to laser peening at cryogenic temperature. Materials Science and Engineering: A, 2018, 734: 291–298.

[17] Liu S Y, Shin Y C. The influences of melting degree of TiC reinforcements on microstructure and mechanical properties of laser direct deposited Ti6Al4V-TiC composites. Materials & Design, 2018, 136: 185–195.

[18] Lin X J, Dong F Y, Zhang Y, et al. Hot-deformation behaviour and hot-processing map of melt-hydrogenated Ti6Al4V/(TiB+TiC). International Journal of Hydrogen Energy, 2019, 44(16): 8641–8649.

[19] Huang X, Gao Y, Wang Z, et al. Microstructure, mechanical properties and strengthening mechanisms of in-situ prepared (Ti_5Si_3+$TiC_{0.67}$)/TC4 composites. Journal of Alloys and Compounds, 2019, 792: 907–917.

[20] Li J X, Wang L Q, Qin J N, et al. Thermal stability of in situ synthesized (TiB+La_2O_3)/Ti composite. Materials Science and Engineering: A, 2011, 528(15): 4883–4887.
[21] Zhang X D, Evans D J, Baeslack W A, et al. Effect of long term aging on the microstructural stability and mechanical properties of Ti-6Al-2Cr-2Mo-2Sn-2Zr alloy. Materials Science and Engineering: A, 2003, 344(1–2): 300–311.
[22] Zhang X D, Bonniwell P, Fraser H L, et al. Effect of heat treatment and silicon addition on the microstructure development of Ti-6Al-2Cr-2Mo-2Sn-2Zr alloy. Materials Science and Engineering: A, 2003, 343(1–2): 210–226.
[23] Li J X, Wang L Q, Qin J N, et al. The effect of heat treatment on thermal stability of Ti matrix composite. Journal of Alloys and Compounds, 2011, 509(1): 52–56.
[24] Zheng Y F, Xu L J, Yu J X, et al. Effect of TiB, TiC and Y_2O_3 on tensile properties and creep behavior at 650 °C of titanium matrix composites. Journal of Alloys and Compounds, 2022, 908: 164699.
[25] Huang S S, Ma Y J, Zhang S L, et al. Influence of alloying elements partitioning behaviors on the microstructure and mechanical properties in alpha plus beta titanium alloy. Acta Metallurgica Sinica, 2019, 55(6): 741–750.
[26] Li J X, Han Y F, Wang L Q, et al. Enhanced ductility of in situ synthesized (TiB+La_2O_3)/IMI834 composite by TRIPLEX heat treatment. Materials Transactions, 2016, 57(10): 1691–1697.
[27] Shi Z F, Guo H Z, Qin C, et al. A method to determine main microstructural features influencing mechanical properties of two-phase titanium alloys. Materials Science and Engineering: A, 2014, 661: 136–141.
[28] Zheng B W, Dong F Y, Yuan X G, et al. Microstructure and tribological behavior of in situ synthesized (TiB+TiC)/Ti6Al4V (TiB/TiC=1/1) composites. Tribology International, 2020, 145: 106177.
[29] Li Y T, Geng L, Xu B, et al. Measurement and analysis of phase transformation temperature of TC11 titanium alloy. Chinese Journal of Rare Metals, 2006, 30(2): 231–235.
[30] Li J X, Wang L Q, Qin J N, et al. Effect of TRIPLEX heat treatment on tensile properties of in situ synthesized (TiB+La_2O_3)/Ti composite. Materials Science and Engineering: A, 2010, 527(21–22): 5811–5817.
[31] Yu J X, Yin Z P, Huang Z R, et al. Effect of aging treatment on microstructural evolution and mechanical properties of the electron beam cold hearth melting Ti-6Al-4V alloy. Materials, 2022, 15(20): 7122.
[32] Jack P, Ammarueda I, Junko U, et al. The effects of heat treatment and carbon content on the microstructure and mechanical properties of laser powder bed fusion Ti-6Al-4V with dissolved TiC particles. Journal of Alloys and Compounds, 2022, 920: 165930.
[33] Ahmed T, Rack H J. Phase transformations during cooling in α+β titanium alloys. Materials Science and Engineering: A, 1998, 243(1): 206–211.
[34] Sun S C, Zhao E T, Hu C, et al. Characteristics of interfacial reactions between Ti-6Al-4V alloy and ZrO_2 ceramic mold. China Foundry, 2021, 18(6): 409–415.
[35] Qi J Q, Wang H W, Zou C M, et al. Temperature dependence of fracture behavior of in situ synthesized TiC/Ti-alloy matrix composite. Materials Science and Engineering: A, 2011, 528(25–26): 7669–7673.
[36] Han Y F, Kuang W, Yang X F, et al. Effect of La and B addition on the microstructure and mechanical properties of titanium matrix composite. Rare Metal Materials and Engineering, 2016, 45(12): 3104–3107.
[37] Boehlert C J, Tamirisakandala S, Curtin W A, et al. Assessment of in situ TiB whisker tensile strength and optimization of TiB-reinforced titanium alloy design. Scripta Materialia, 2009, 61(3): 245–248.
[38] Wang S, Huang L J, An Q, et al. Regulating crack propagation in laminated metal matrix composites through architectural control. Composites: Part B, 2019, 178: 107503.
[39] Zhang W, Zhou S Q, Ren W J, et al. Tailoring strength-ductility of titanium matrix composites reinforced with graphene nanoplatelets. Materials Science and Engineering: A, 2022, 861: 144386.
[40] Li C J, Fu B G, Dong T S, et al. Microstructure and dry sliding wear behavior of as-cast TiC_p/Ti-1100-0.5Nb titanium matrix composite at elevated temperatures. China Foundry, 2021, 18(6): 455–463.
[41] Gorunov A I. Wear-resistant carbon-fiber-reinforced Ti-based composite obtained by laser metal deposition. Journal of Materials Engineering and Performance, 2020, 29(5): 3305–3314.
[42] Cho C W, Lee Y Z. Effects of oxide layer on the friction characteristics between TiN coated ball and steel disk in dry sliding. Wear, 2003, 254(3–4): 383–390.
[43] Vajdi M, Moghanlou F S, Ahmadi Z, et al. Thermal diffusivity and microstructure of spark plasma sintered TiB_2-SiC-Ti composite. Ceramics International, 2019, 45(7): 8333–8344.
[44] Lin G, Peng Y, Li Y, et al. Remarkable anisotropic wear resistance with 100-fold discrepancy in a copper matrix laminated composite with only 0.2 vol% graphene. Acta Materialia, 2021, 215: 117092.
[45] Dong H Y, Wu K M, Wang X L, et al. A comparative study on the three-body abrasive wear performance of Q&P processing and low-temperature bainitic transformation for a medium-carbon dual-phase steel. Wear, 2018, 402: 21–29.
[46] Li J X, Han Y F, Yang D Y, et al. Effect of heat treatment on creep properties of in situ synthesized (TiB+La_2O_3)/Ti composite. Frontiers in Materials, 2019, 6: 103389.
[47] Li H L, Jia D C, Yang Z H, et al. Achieving near equiaxed alpha-Ti grains and significantly improved plasticity via heat treatment of TiB reinforced titanium matrix composite manufactured by selective laser melting. Journal of Alloys and Compounds, 2020, 836: 155344.
[48] Eivani A R, Valipour S, Ahmed H, et al, Effect of the size distribution of nanoscale dispersed particle on the Zener drag pressure. Metallurgical and Materials Transactions A, 2011, 42A(4): 1109–1116.
[49] Zheng Z Z, Kong F T, Wang X P. The α phase recrystallization mechanism and mechanical properties of a near-α titanium matrix composite. Intermetallics, 2022, 147: 107597.
[50] Xu W, Brandt M, Sun S, et al. Additive manufacturing of strong and ductile Ti-6Al-4V by selective laser melting via in situ martensite decomposition. Acta Materialia, 2015, 85: 74–84.
[51] Wang J H, Guo X L, Qin J N, et al. Microstructure and mechanical properties of investment casted titanium matrix composites with B_4C additions. Materials Science and Engineering: A, 2015, 628: 366–373.
[52] Tabrizi S G, Babakhani A, Sajjadi S A, et al. Microstructural aspects of in-situ TiB reinforced Ti-6Al-4V composite processed by spark plasma sintering. Transactions of Nonferrous Metals Society of China, 2015, 25(5): 1460–1467.
[53] Lu W J, Guo X L, Meng J L, et al. Analysis of the coupling effects of tib whiskers and tic particles on the fracture toughness of (TiB+TiC)TC4 composites: Experiment and modeling. Metallurgical and Materials Transactions A, 2015, 46(8): 3490–3501.
[54] Lu W J, Guo X L, Meng J L, et al. Analysis of the coupling effects of TiB whiskers and TiC particles on the fracture toughness of (TiB+TiC)/TC4 composites: Experiment and modeling. Metallurgical and Materials Transactions: A, 2015, 46(8): 3490–3501.